

Laboratory experiments of wave interaction with submerged oscillating bodies[†]

Linda Eckel and Masoud Hayatdavoodi

Abstract—This study is concerned with laboratory experiments of interaction of nonlinear water waves with submerged, oscillating bodies in shallow water. Due to the propagation of surface waves, time-dependent pressure differential is formed above and under the submerged body. This pressure differential results in oscillatory vertical force on the body. A vertical, thin guide rail, attached to the tank floor and extended to the free surface, is used to allow the object to oscillate in the vertical direction and restricts motions in other directions. Oscillations of the object is controlled by a spring. A range of wave conditions are considered by changing the wave period and wave height. Submerged objects used in these experiments include a circular disc and a three-dimensional cone-shape body. Several springs with different stiffness are considered in this study. The wave-induced oscillations of the objects are recorded by a camera and data are recorded and processed as time-varying oscillations of the object. Discussion is provided on to the change of acceleration and oscillation height of the object under various wave conditions and spring stiffness. A vertically submerged disc or cone is the core component of a fully submerged wave energy device in shallow water. Mechanical oscillation of the submerged body is converted into electricity by using a direct-drive power take-off system. A submerged oscillating body also acts as a wave breaker, mitigating the severity of waves approaching shorelines. The wave transformation above the oscillating body is recorded by several wave gauges upwave and downwave of the body and results are compared and discussed.

Keywords—Submerged disc, Wave energy device, Wave-structure interaction, Oscillating body

I. INTRODUCTION

At the time of the worldwide rising energy consumption the extraction of new energy resources is one of the most challenging tasks for engineers and scientists. Our life is impacted by the energy consumption such as electricity or thermal energy. The electricity consumption is driven on one hand by the growing population and on the other by the increasing consumption per person. At the same time, the high energy demand covered by fossil fuels leads to the release of global warming gases which cause the climate change. Therefore it is essential to develop and use sustainable energies. One possibility of this sustainable energy extraction are marine renewable energies.

[†]The 13th European Wave and Tidal Energy Conference, EWTEC2019, 1-6 September, 2019, Napoli, Italy.

Paper ID: 1799, Track: Wave hydrodynamic modelling

L. Eckel is with the Mechanical Engineering Department of the Universitaet der Bundeswehr Muenchen, Muenchen, 80799, Werner-Heisenberg-Weg, Germany (e-mail: Linda.Eckel@unibw.de).

M. Hayatdavoodi is with the Marine Hydrodynamics and Ocean Engineering of Civil Engineering Department, School of Science and Engineering, University of Dundee, Dundee, DD1 4HN, UK (e-mail: MHayatdavoodi@dundee.ac.uk).

According to a study by the World Energy Council in 2013 [1], the global energy requirements in 2020 will be covered by 18% renewable energies and by 76% of fossil energies. The study predicts an increase of 5% in the share of renewable energies compared to 2011. Nevertheless, renewable energies represent only a small part of the energy supply. Oceans and seas are a possible source of marine renewable energies.

Due to this large energy capacity, which is many times greater than the global electricity demand, oceans play an important role in the implementation of climate targets[2].

Until now, this energy source has hardly been used, mainly due to various technical and economic challenges that this kind of projects deal with. One of these possible regenerative technologies is through the use of Wave Energy Converter (WEC). WEC are systems that convert the kinetic energy of waves into usable electricity.

This wave energy has the highest energy density among renewable resources, see e.g.[3]. Since wave energy has rarely been used so far [4], it offers extensive possibilities. Especially the coasts of Great Britain and France are large sea areas whose wave energy can be used[3]. However, discussed by [3], many projects are still in the R&D stage and are not yet fully developed.

Various challenges in development of practical WEC include (i) complex operational mechanism, (ii) large loads due to wave breaking on the structures, (iii) variant device performance under different wave directions in oceans, and (iv) the visual impact of the energy devices, which is not desirable.

In response to some of these challenges, a new wave energy device concept has been introduced by [5]. This device consists of a fully submerged oscillating body, which operates in all wave directions. The proposed device consists of a horizontal body (disc or wedge) connected to a direct-drive power take-off (PTO) system. The device frame is fixed on the seafloor. The body is allowed to oscillate in the vertical direction over guide rails (while other motions are restricted) due to the interaction of water waves. The submerged device has a simple geometry and mechanism, it's performance is invariant with the wave direction, and it is protected from the impact of the extreme wave loads on the surface

Nonlinear wave loads on submerged horizontal discs of WEC have been studied by, for example, [6], [7]. Theoretical and computational analysis of wave-induced oscillations of submerged discs are discussed in [8], [9]. Structural analysis of the proposed submerged wave energy device are given in [10] and [11]. Aside from the direct application of submerged horizontal discs to the proposed wave energy device, submerged discs have been used as the core component of several other wave energy devices, see e.g., [12], [13], [14], [15], for various applications. A theoretical analysis of submerged oscillating

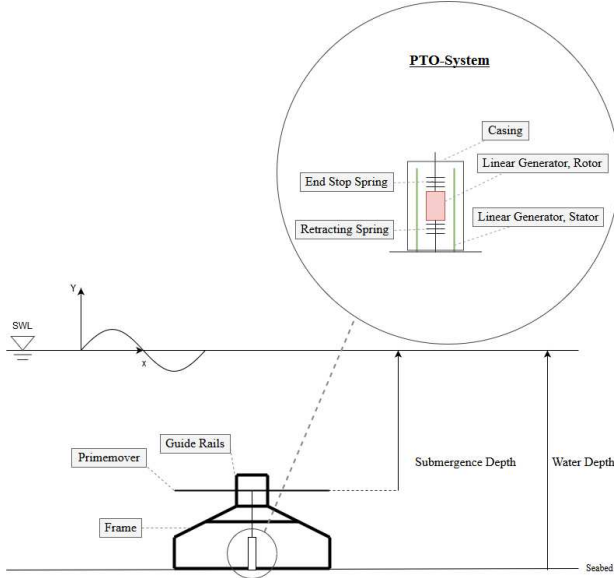


Fig. 1. Schematic of the submerged Wave Energy Device.

discs as a wave breaker is given by [16]. Theoretical and experimental studies of waves generated by an oscillating circular cylinder in water of finite depth is presented by [17].

This study is concerned with laboratory experiments of wave interaction with submerged oscillating bodies. The goal of these experiments are to study the oscillation of submerged objects due to the wave impact, and to analyse the effect. Particular attention is given to the determination of the wave-induced motion of submerged bodies under various wave conditions and control systems. Intermediate and shallow water conditions are considered. Results are presented in the form of the oscillation height of the bodies and surface elevations.

In section II, the particular wave energy device under consideration is introduced. This is followed by experimental design, and results and discussion in section III and IV, respectively. The paper is closed with concluding remarks in section V.

II. REVIEW OF THE WAVE ENERGY DEVICE

A concept design of the submerged oscillating heaving device is shown in Fig. 1.

The WEC works as follows: The prime mover is submerged in shallow water, under the surface. Motion of the prime mover is restricted by use of guide rails. As only a vertical movement of the prime mover is allowed, it is a heaving device. The frame is fixed to the seafloor, and it holds the device on the seabed. The prime mover moves vertically up and down on four guided rails of the frame. This prevents horizontal deviation or rotation of the prime movers. The prime mover is connected to the PTO system. This design consists of a linear generator, with the stator firmly anchored and the rotor connected to the prime mover. The rotor is connected to a spring, which causes a restoring force, see e.g.[18]. Further details of this wave energy device can be found in [5].

With the vertical oscillations of the prime mover, power is generated by the linear generator. The power

generation depends on the oscillation's velocity and thus the movement of the prime mover. This leads to a challenging problems of WEC's, control of the power generation. In this system, a spring is attached to the oscillations of the prime mover. Along with the damping effect of the linear power take-off, the spring is used to control the oscillations.

The power output, P , depends on the wave condition, wave height H and wave period T , the water depth h , the shape and the size of the prime mover, as well as the submergence depth s , the bearing friction coefficient μ and the spring stiffness k . This is shown in (1):

$$P = f(H, T, h, \text{shape, size, } s, \mu, k). \quad (1)$$

The function f is unknown. The goal of this study is to provide some information about this function by conducting laboratory experiments. Attention is confined to the oscillation of the prime mover, attached to a spring, under various environmental conditions. That is, we are interested in determining the wave-induced oscillation of submerged bodies with different shapes, under various wave conditions and spring stiffness. Effects of the PTO, which appears in form of a damping load, is not considered in these laboratory experiments.

III. EXPERIMENTAL DESIGN

Laboratory experiments are conducted on small-scale (between 1:15 - 1:30, depending on the water depth) model of oscillating bodies. Various submerged objects, springs and wave conditions are considered. The goal of these experiments is to study the wave-induced oscillations of the submerged bodies under various load conditions. The laboratory experiments are discussed in this section. Further information about the experiments can be found in [19].

Facilities and instrumentation

The laboratory experiments are conducted in the Fluid Mechanics Laboratory of the School of Science and Engineering of the University of Dundee. A schematic of the experimental setup is shown in Fig. 2.

The experiments are carried out in a wave flume, 12 m long, 0.6 m wide, and 0.6 m height. On the left side of the tank, the waves are generated by a piston wave maker to simulate shallow water. See [20], for a discussion on various types of wave maker and their applicability to different wave conditions.

At the right end of the wave tank, the waves are captured by a wave absorber. This wave absorber, approximately 1.5 m long, is designed to prevent reflection of waves back into the tank. The movement of the wave through the tank is detected by three wave gauges. Gauge one is located at a distance of 2.1 m from the wave maker. The following two wave gauges are placed at 1.5 m downwave from each other, see Fig. 2. Throughout the experiments, water depth is kept constant a $h = 30 \text{ cm}$. All three gauges are mounted vertically at half the width of the wave tank.

In this experimental setup, the test object is located half way between Gauge 1 and 2 and is driven by a linear bearing on a fixed shaft in vertical position, Fig. 3. A spring is attached to the linear bearing to control the motion. On top, the spring is attached to the shaft,

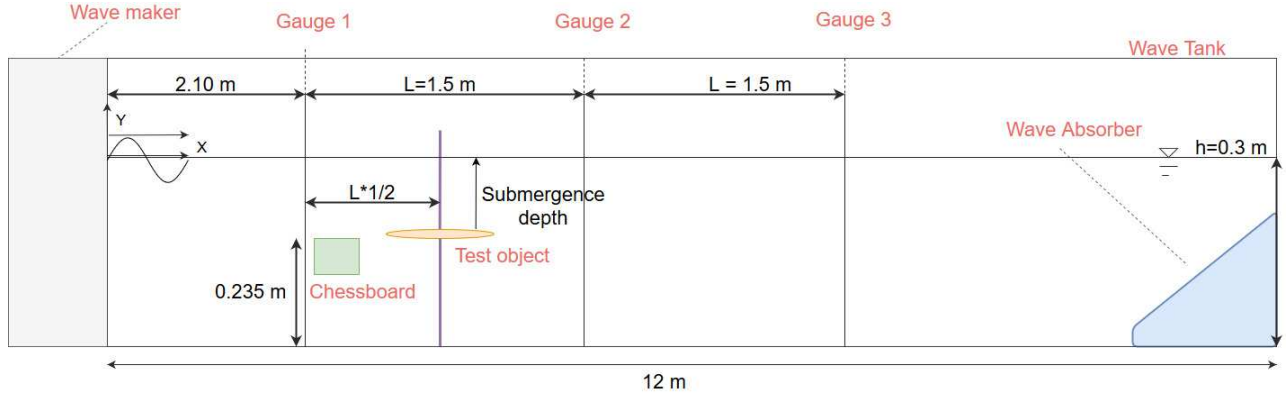


Fig. 2. Schematic of the experimental wave tank, and location of the wave gauges.

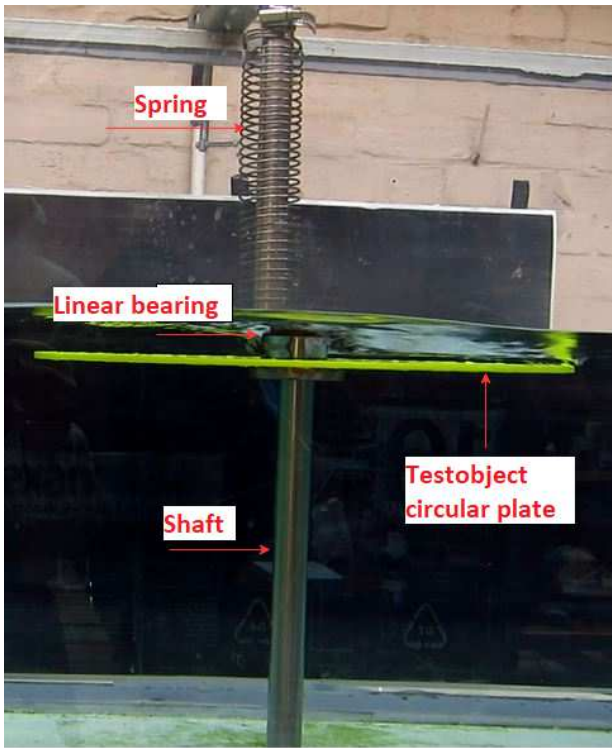


Fig. 3. Structure of the circular object, attached to the linear bearing, which can oscillate on the vertical shaft due to the wave loads. The spring is connected to the linear bearing.

see Fig. 3. The PTO has a damping effect and is not considered in these experiments.

A. Measurements and data processing

During the experiments, the generated waves are recorded as well as the oscillation of the test objects. While the test objects are detected by video analysis, the wave surface elevation is recorded by wave gauges. The wave gauges are capacitance-type (wave staff XB manufactured by Ocean Sensors) with sampling frequency of 30 Hz and 0.1% accuracy.

The calibration of the wave gauges are carried out by measuring points in the range of 20–80% of the expected measuring range of the water surface. Each calibration point has a tolerance of 0.05%. During calibration, a

voltage value is assigned to each measuring point at a known water depth. This creates a calibration line that is stored and called up in the system. The wave gauges used here are limited to maximum 50 cm water depths.

The movement of the test objects, a circular disc (Object 1) and a cone (Object 2), is detected by a camera located in approximately 1.5 m away from the wave tank. A set of video calibration, image processing, object detection and motion recording steps are carefully followed to detect the oscillations. These are discussed here: To determine the coordinate system at all times, and hence the relative camera position and angle of the oscillating of the test object, a checkerboard is fixed to the tank wall.

First, calibration images of the checkerboard are determined from different angles. Together with the size of the checkerboard cells, the Matlab program *Camera-Calibration* identifies the origin of the coordinate system to determine the position of the test objects. In these experiments, the origin is located 0.22 m above the tank bottom. This defines the absolute movement in the water. The camera distortion and camera properties are then determined in the program to describe how the camera creates correctly-sized 2D image from a 3D environment. This is important in order to later deduce the 3D reality from the images and thus to calculate the actual position of the test objects in the tank.

The video recordings of the experiments are analysed in a specially developed program called *MotionTracker2*. This program works in Matlab and base on a color separation algorithm. Then, the movement of the colored test objects is determined in the tank. In the first step, the video data are read, as frames per seconds. The video is then saved in its image sequence. These images are then analysed for the position of the object at each frame. The video information allows each image to be assigned to a specific point in time.

The image analysis process to determine the location of the object is discussed here. First, the color values of the pixels of each individual image are queried in the analysis. The information of the color values can be presented in different formats. Therefore, we first determine which type of the color information exists and if necessary, convert into a true-color format. A true color images characterizes each color with three values, by describing the terms of the color amount of red, green, and blue. Next, the color values are converted to HSV

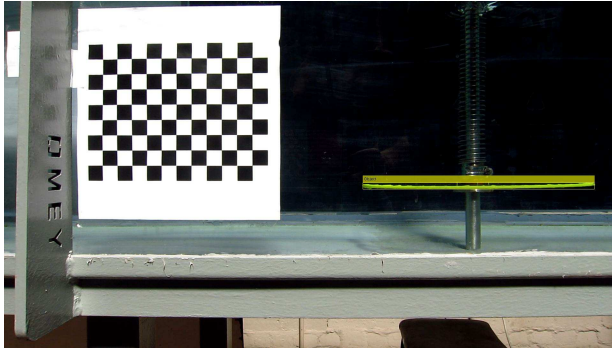


Fig. 4. Test object circular plate after analysis with the *Motion-Tracker2*. The detected object is framed by the program with a yellow box.

format. HSV describes colors using three values for hue, saturation and value. HSV is always preferred when a colour description is required. The reason for this is that the HSV model is more similar to the human visual perception and therefore easier to define and select colour value ranges. Since the user should later be able to adjust these ranges for different recording conditions, a color description is necessary. See [21] for more details.

Once the above is accomplished, the HSV values are written into a corresponding matrix (*hImage*, *sImage* and *vImage*) according to hue, saturation and value. The desired colors in each image are then detected by defining threshold values for the HSV. In the next step, all values in these three matrices, which are in the desired color value range, are transferred to three new matrices (*hueMask*, *saturationMask* and *valueMask*). If values are not in the value range, they are stored as zeros in the new matrices.

Now the three matrices *hueMask*, *saturationMask* and *valueMask* are combined again as *colorObjectMask*. If all three HSV properties have a value for one pixel, they describe the color we are looking for. If only one of these three values is zero, the pixel is not included in the detection.

With the help of the command *blobAnalysis* the contiguous pixel area is captured by coordinates and provided with a box. Then the areas are sorted by size and the largest detected area is used for further steps. In the original image a box is then inserted around the pixel area and the coordinates of the detected area are corrected with the camera parameters, see Fig. 4.

B. Model specimen and setup

Two test objects are used in this study. Test object one is a circular plate made of Plexiglas, shown in Fig. 5. It has a diameter of 30 cm and a thickness of 3 mm. The object is prepared with a linear bearing in the center to guide it later on a vertical fixed shaft. It therefore has a central circular opening for the type of a *LMF20UU* bearing and can hold a shaft with a diameter of 20 mm. Bearing and shaft are connected by a spring. The test object with the bearing and the screws weigh 432 g. The friction coefficient between the bearings amounts and the shaft is $\mu = 0.0048$.

In order to capture the transparent material with the video camera, a part of the edge is covered with bright coloured adhesive tape.

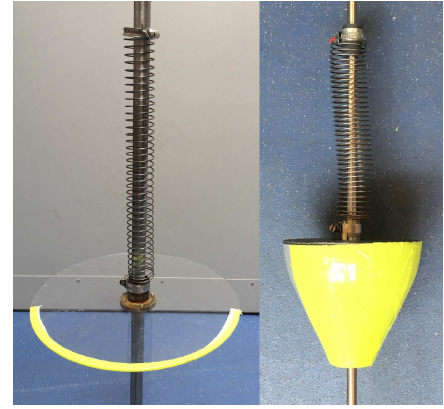


Fig. 5. Test objects. Left side test object one, the circular plate, and right side test object two, the cone.

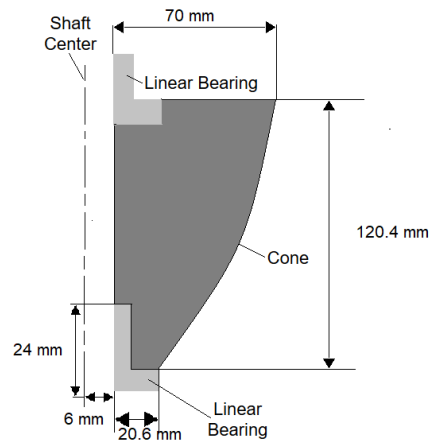


Fig. 6. A CAD drawing of the test object cone.

The second test object is an optimized 3D cone. The hydrodynamic design is based on the Berkeley Wedge concept, see [22]. This research deals with an optimal shape of asymmetric prime movers on the water surface which are used in heaving WEC with linear generators. The form function of the Wedge in [22] is given by

$$F(\bar{y}) = \bar{x} = 0.05926(\bar{y} + 1)^2 + 3.88147(\bar{y} + 1)^3 - 2.94074(\bar{y} + 1)^4. \quad (2)$$

\bar{x} and \bar{y} are dimensionless coordinates as given by

$$\bar{x} = x/b, \quad \bar{y} = y/D, \quad (3)$$

where b is the maximum width of the object in x direction for $x < 0$ and D is the draft of the object in y direction for $y < 0$.

Further conditions for the form function result from constructive and experimental limitations. These include the integration of the bearings *LMF10UU* as shown in Fig. 6. The result is a truncated cone. The shape function for the height $|D|$ goes up to $x = 0$, so the real height D^* is introduced so that only a part of function is considered. This real height D^* depends on the flange radius r_F of the bearing. This results in these functions:

limits, depending on r_F and b :

$$[-b, -r_F) = [-b, -r_F] := x \in R \mid -b \leq x < -r_F. \quad (4)$$

However Eq. (2) is depending on D and b . Hence D and b are selected in such that the cone dimensions do not exceed the dimensions of the wave tank, while the real height D^* is as large as possible and a pointed truncated cone is formed. Therefore, $b = 70 \text{ mm}$, $r_F = 20.5 \text{ mm}$ and $D = 230 \text{ mm}$ were chosen. This results in $D^* = 118.6 \text{ mm}$ and the new form function (5). If Eq. (5) is rotated around the y-axis, a truncated cone is created:

$$F(y) = x = 70 * [0.05926(\frac{y}{230} + 1)^2 + 3.88147(\frac{y}{230} + 1)^3 - 2.94074(\frac{y}{230} + 1)^4]. \quad (5)$$

After modelling the outer shape of the cone, the wall thicknesses are modelled. A CAD model was developed from these form conditions and then the object was created using a 3D printer.

As the prime mover should float in the water and only be moved by the force of the water motion, the required weight is calculated by the Archimedean principle. The material density and the displacement volume from the CAD data were used for this purpose. The missing weight was attached to the top of the model in form of a 2 mm thick circular metal plate, Fig.5. To prevent the cone from absorbing water when submerged, it was painted and silicone was used to seal the top and bottom connections and the screws. The final weight of the cone, including the attached linear bearing, was recorded at $m_c = 971 \text{ g}$. The cones weight was measured before and after the experiments. A change in mass of maximum 3.5% was measured through out the experiments due to water absorption or alike.

We note that initially the cone was designed to operate with two linear bearings on the top and the bottom parts, showing in Fig. 6. During the experiments, however, it was determined that any small change in the alignment of the linear bearings an the shaft results in resting forces that would significantly impact the oscillations. It is not possible to measure this resting force (which is due to misalignment) and hence one of the bearings (the bottom bearing, Fig. 6) was removed, i.e. the cone hold in place with one linear bearing.

For the experiments two different springs were used. The springs were custom-made for these experiments. The initial lengths of the springs 1 and 2 are 18.8 cm and 22.6 cm , respectively. The springs stiffness were determined through a static analysis. This was accomplished by adding weight (14 different values) to the springs and carefully measured the change in length. Results are shown in Fig. 7. The spring 1 and 2 stiffness were determined as $K_1 = 35.7 \text{ N/m}$ and $K_2 = 28.7 \text{ N/m}$, respectively. Simplified, design-type equations for wave-induced forces on submerged discs can be found in [23].

C. Experimental procedure

The laboratory experiments are carried out with different models, spring and wave conditions. Water depth is kept constant at $h = 0.3 \text{ m}$ throughout the experiments. A range of wave conditions is considered to cover nonlinear intermediate- and shallow-water waves: $\frac{h}{gT^2} < 0.06$ and

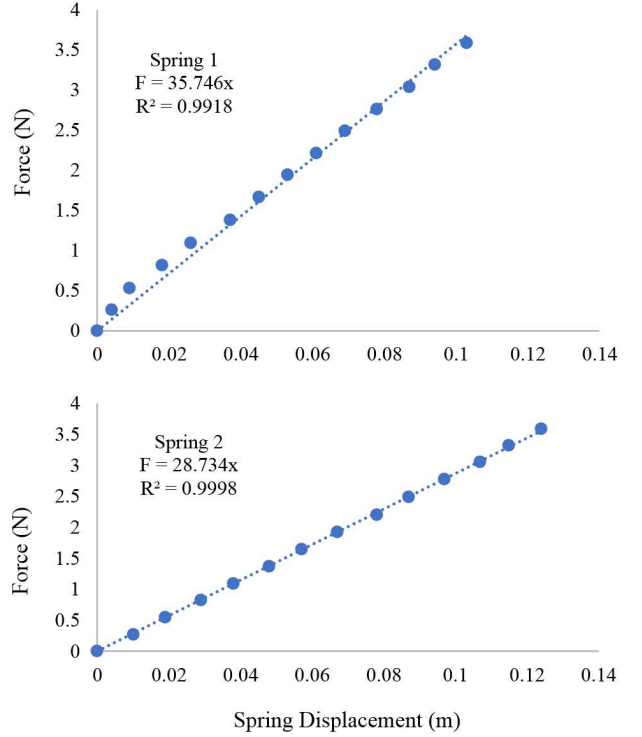


Fig. 7. Results of the stiffness tests of the two springs. The circular markers are the measured values, and the dashed lines are the fitted line. Also shown on the figure is the R-squared value; very close to 1.0 in both cases.

TABLE I.
DIMENSIONLESS EXPERIMENTAL PARAMETERS.

\bar{H}	\bar{T}
$\bar{H}_1 = 0.034$	$\bar{T}_1 = 4$
$\bar{H}_2 = 0.067$	$\bar{T}_2 = 5.72$
$\bar{H}_3 = 0.1$	$\bar{T}_3 = 7.15$
$\bar{H}_4 = 0.134$	$\bar{T}_4 = 8.58$
$\bar{H}_5 = 0.167$	$\bar{T}_5 = 10$
$\bar{H}_6 = 0.2$	—

$\frac{H}{gT^2} > 0.0017$, (see, for example, [24]) for the cases considered here.

In Table I, the parameters are given in dimensionless form by:

$$\bar{T} = \frac{T}{\sqrt{h}}, \quad \bar{H} = \frac{H}{h}, \quad (6)$$

where T is the wave period and H is the wave height. This results dimensioned in the following test parameters shown in Table II, for $h = 0.3 \text{ m}$.

Experiments are conducted for various initial submer-

TABLE II.
EXPERIMENTAL PARAMETERS.

H[mm]	T[s]	IS [mm]
$H_1 = 10$	$T_1 = 0.70$	$IS_0 = 300$
$H_2 = 20$	$T_2 = 1.00$	$IS_1 = 270$
$H_3 = 30$	$T_3 = 1.25$	$IS_2 = 210$
$H_4 = 40$	$T_4 = 1.50$	$IS_3 = 150$
$H_5 = 50$	$T_5 = 1.75$	$IS_4 = 90$
$H_6 = 60$	—	—

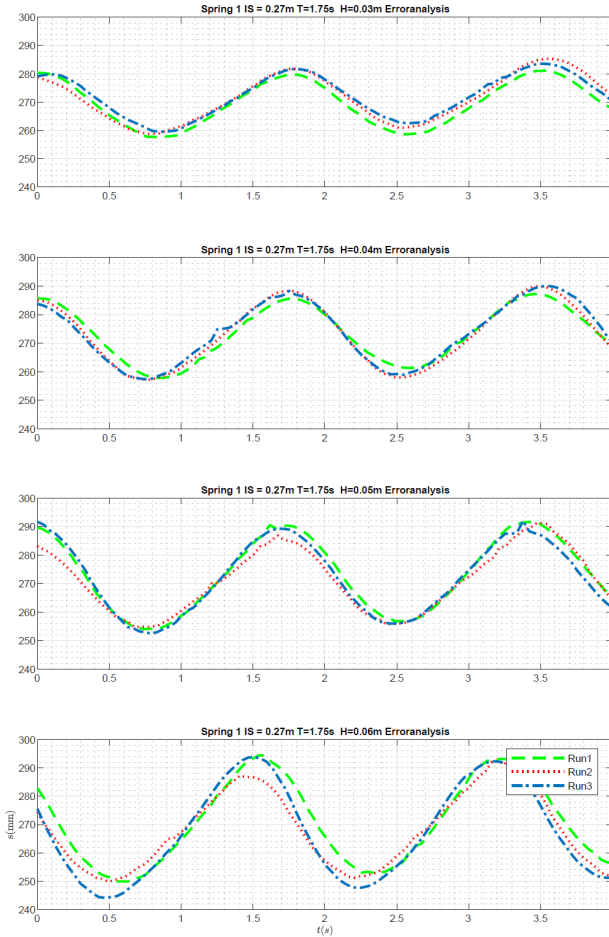


Fig. 8. Time series of the circular disc oscillations for the error analysis. The horizontal axis shows the time (in seconds) and the vertical axis is the disc oscillations (in millimeters). The initial submergence depth ($IS = 0.27$) and the wave period ($T = 1.75$) are kept constant, while wave height is variable $H = 0.03\text{ m}, 0.04\text{ m}, 0.05\text{ m}$ and 0.06 m from top to bottom sub-figures, respectively. Spring one is used in this study.

gence depth, IS , defined as the distance from the tank floor to the upper edge of the object. Test object one was tested with both springs and all various wave heights, waver periods and submergence depths 1 to 4. Whereas the experiments with test object two were done for all periods, but only with spring two and wave height H_6 , for the submergence depths IS_0 and IS_1 .

The water density ρ is constant during the experiments and is 997 kg/m^3 .

D. Error analysis

To determine the repeatability error of the experiments, the wave conditions were repeated three times for test object one with spring one and for all submergence depths.

The oscillation height of the test object, H_{oz} , for all three repetitions has been determined. Sample time series of the three repeats of disc oscillations under various wave conditions is shown in Fig. 8 for fixed period ($T = 1.00\text{ s}$) and submergence depth ($IS = 1.25$) and variable wave height.

The deviation of the oscillation height from the average is calculated. This is referred here as oscillations height deviation $H_{oz,error}$:

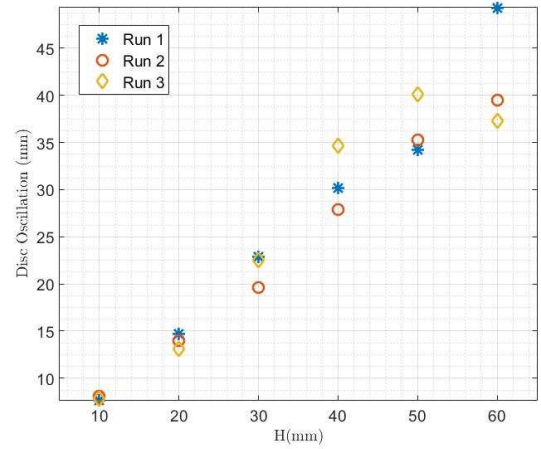


Fig. 9. Variation of the disc oscillations with wave height for the three repeated tests of the error analysis. Spring one, submergence $IS = 0.27\text{ m}$ and wave period $T = 0.70\text{ s}$.

TABLE III.
PERCENTAGE ERRORS OF DISC OSCILLATIONS AFTER THREE REPEATED TESTS OF THE ERROR ANALYSIS STUDY. SPRING 1, SUBMERGENCE DEPTH $IS = 0.27\text{ m}$.

H [mm]	T [s]	0.70	1.00	1.25	1.50	1.75
		36.6	7.8	3.2	—	—
10	2.7	12.9	4.5	7.9	32.3	
20	6.1	16.8	2.5	14.3	9.7	
30	21.7	27.1	12.6	14.2	19.1	
40	22.6	19.2	17.0	9.3	6.6	
50	12.5	31.5	10.9	4.3	25.4	
60						

$$H_{oz,error} = \frac{H_{oz,max} - H_{oz,min}}{H_{oz,Average}} * 100\%, \quad (7)$$

where $H_{oz,max}$ and $H_{oz,min}$ are the largest and smallest oscillation height, respectively, of the three repeats. $H_{oz,Average}$ is the average body oscillation for the conditions. Sample results of the disc oscillation heights repeated in three tests of the error analysis study are shown in Fig. 9. Sample results of the calculated errors are given in Table III.

The repeatability error range for the oscillation height is large. On the whole, no correlations of the error $H_{oz,error}$ between the individual submergence depths can be observed. About 90% of the oscillation height repeatability errors are in the range of 4–20%. However, per submergence depth are about 2–4 values that exceed this range. In very few cases, the oscillation height error is twice the mean oscillation height.

Due to the large scattering range of the repeatability error deviations, the standard deviations of the oscillations are calculated by:

$$\tilde{s} = \sqrt{\frac{\sum_{i=1}^3 (H_{n,oz,i} - H_{n,oz,Average})^2}{3}} \quad (8)$$

The index n , used there, denotes the wave height H of 1–6. The results are given in Table IV. This means

TABLE IV.
ERROR ANALYSIS, STANDARD DEVIATION OF THE OSCILLATION HEIGHT $H_{OZ,SD}$ (mm) SPRING 1, $IS = 0.27\text{ m}$ WITH THE TEST OBJECT CIRCULAR PLATE.

H [mm]	T [s]				
	0.70	1.00	1.25	1.50	1.75
10	0.648	2.772	1.603	-	-
20	0.141	1.667	0.869	2.386	2.108
30	0.450	2.536	2.941	2.863	1.597
40	2.176	6.511	1.910	3.285	3.844
50	2.532	6.341	3.581	5.043	5.453
60	1.715	6.533	2.331	0.805	4.705

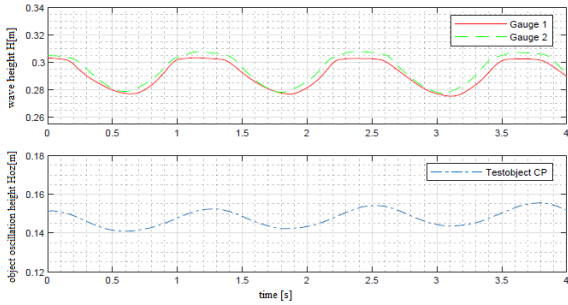


Fig. 10. Time series of surface elevation and disc oscillation, spring one, $IS = 0.27\text{ m}$, $T = 1.75\text{ s}$ and $H = 0.03\text{ m}$.

that the average oscillation heights vary between 0.1 and 6.5 mm.

In general, increasing wave height results in larger error, while wave period does not seem to have a direct impact. Further information on the error analysis can be found in [19].

IV. RESULTS AND DISCUSSION

Results of the experiments are presented in this section. Figure 10 shows time series of oscillation of the circular disc, and the surface elevation recorded at Gauge I and II. Oscillation heights are recorded for all test cases, and these are given in Tables V to XII.

The experiments with test shape circular plate have shown the following behaviour with both springs:

With rising submergence depth a decrease of the oscillation height is to be observed, whereby the values for submergence depth s_4 deviate more clearly than the remaining submergence depths. Within a submergence depth, the oscillation height increases with increasing wave height. In general, an increasing object oscillation H_{oz} can also be observed with increasing period, although some measured values deviate from this behaviour. The measured values of the period $T = 1.25\text{ s}$ are particularly frequently affected. Another point of the oscillation behaviour is the movement behaviour of the test object, which is gentler than the wave. This means that with a rush of the wave, the object follows smooth oscillation. This is due to spring force.

To compare the behaviour of the test object with different springs, similar oscillation heights are obtained:

- Spring one:

- s_1 : $H_{oz}/h = 0.015 - 0.15$
- s_2 : $H_{oz}/h = 0.014 - 0.13$
- s_3 : $H_{oz}/h = 0.007 - 0.073$

TABLE V.
RATIO OF WAVE HEIGHT TO OSCILLATION HEIGHT, H_{OZ}/H OF THE TEST OBJECT 1 SPRING 1 $IS = 0.27\text{ m}$.

H [mm]	T [s]				
	0.70	1.00	1.25	1.50	1.75
10	0.016	0.027	0.015	-	-
20	0.037	0.049	0.047	0.040	0.057
30	0.060	0.076	0.076	0.084	0.063
40	0.067	0.093	0.100	0.102	0.097
50	0.102	0.118	0.115	0.143	0.111
60	0.109	0.124	0.122	0.143	0.154

TABLE VI.
RATIO OF WAVE HEIGHT TO OSCILLATION HEIGHT, H_{OZ}/H OF THE TEST OBJECT 1 SPRING 1 $IS = 0.21\text{ m}$.

H [mm]	T [s]				
	0.70	1.00	1.25	1.50	1.75
10	0.014	0.021	0.014	-	-
20	0.025	0.038	0.038	0.033	0.032
30	0.037	0.055	0.055	0.060	0.056
40	0.049	0.079	0.068	0.072	0.074
50	0.067	0.090	0.075	0.088	0.079
60	0.083	0.111	0.084	0.091	0.130

- s_4 : $H_{oz}/h = 0.004 - 0.042$
- Spring two:
 - s_1 : $H_{oz}/h = 0.02 - 0.15$
 - s_2 : $H_{oz}/h = 0.012 - 0.098$
 - s_3 : $H_{oz}/h = 0.006 - 0.077$
 - s_4 : $H_{oz}/h = 23*10^{-5} - 41*10^{-4}$

Considering all values of one submergence depth, the oscillation height, with the stronger spring one, is generally higher than with spring two. This behaviour is shown in the Tables V to IX. As result of the close spring stiffness the measured values are also close to each other. Deviations of the addressed behaviour could be related to measurement errors.

The behaviour of test object two was only tested with spring two and wave height H_6 and results are given in Tables XIII and IV. A decline in the association of objects can be observed with increasing submergence depth too. The oscillation behaviour of a continuously submerged test object with increasing submergence depth must be investigated by further tests.

An increase in oscillation with the period can only be observed for IS_0 , however, when viewing the videos a stuttering oscillation is visible, which is obviously caused by friction of the tilting bearing. Due to the limited test of the object, these tests could not be repeated. Based on

TABLE VII.
RATIO OF WAVE HEIGHT TO OSCILLATION HEIGHT, H_{OZ}/H OF THE TEST OBJECT 1 SPRING 1 $IS = 0.15\text{ m}$.

H [mm]	T [s]				
	0.70	1.00	1.25	1.50	1.75
10	0.007	0.013	0.010	-	-
20	0.012	0.022	0.024	0.021	0.019
30	0.019	0.035	0.033	0.041	0.037
40	0.029	0.045	0.042	0.057	0.048
50	0.039	0.055	0.049	0.059	0.068
60	0.040	0.064	0.058	0.064	0.073

TABLE VIII.
RATIO OF WAVE HEIGHT TO OSCILLATION HEIGHT, H_{OZ}/H OF THE TEST OBJECT 1 SPRING 1 $IS = 0.09\text{ m}$.

H [mm] \ T [s]	0.70	1.00	1.25	1.50	1.75
10	0.004	0.007	0.007	—	—
20	0.008	0.016	0.017	0.017	0.020
30	0.010	0.021	0.021	0.028	0.020
40	0.014	0.026	0.026	0.035	0.031
50	0.019	0.033	0.037	0.042	0.037
60	0.023	0.039	0.038	0.042	0.041

TABLE IX.
RATIO OF WAVE HEIGHT TO OSCILLATION HEIGHT, H_{OZ}/H OF THE TEST OBJECT 1 SPRING 2 $IS = 0.27\text{ m}$.

H [mm] \ T [s]	0.70	1.00	1.25	1.50	1.75
10	0.020	0.029	0.018	—	—
20	0.034	0.047	0.047	0.044	0.046
30	0.059	0.067	0.068	0.088	0.073
40	0.082	0.088	0.090	0.107	0.091
50	0.081	0.103	0.112	0.125	0.124
60	0.103	0.123	0.127	0.153	0.122

TABLE X.
RATIO OF WAVE HEIGHT TO OSCILLATION HEIGHT, H_{OZ}/H OF THE TEST OBJECT 1 SPRING 2 $IS = 0.21\text{ m}$.

H [mm] \ T [s]	0.70	1.00	1.25	1.50	1.75
10	0.012	0.019	0.013	—	—
20	0.018	0.035	0.044	0.034	0.035
30	0.031	0.055	0.054	0.056	0.061
40	0.049	0.067	0.071	0.092	0.069
50	0.054	0.086	0.070	0.091	0.086
60	0.070	0.098	0.079	0.094	0.090

TABLE XI.
RATIO OF WAVE HEIGHT TO OSCILLATION HEIGHT, H_{OZ}/H OF THE TEST OBJECT 1 SPRING 2 $IS = 0.15\text{ m}$.

H [mm] \ T [s]	0.70	1.00	1.25	1.50	1.75
10	0.006	0.014	0.006	—	—
20	0.012	0.023	0.026	0.021	0.029
30	0.019	0.034	0.034	0.036	0.042
40	0.025	0.045	0.046	0.060	0.057
50	0.030	0.055	0.055	0.061	0.067
60	0.036	0.069	0.063	0.072	0.077

TABLE XII.
RATIO OF WAVE HEIGHT TO OSCILLATION HEIGHT, H_{OZ}/H OF THE TEST OBJECT 1 SPRING 2 $IS = 0.09\text{ m}$.

H [mm] \ T [s]	0.70	1.00	1.25	1.50	1.75
10	0.002	0.007	0.004	—	—
20	0.005	0.015	0.014	0.016	0.014
30	0.009	0.019	0.017	0.023	0.023
40	0.013	0.027	0.024	0.030	0.028
50	0.017	0.031	0.029	0.034	0.035
60	0.020	0.038	0.033	0.038	0.041

TABLE XIII.
RATIO OF WAVE HEIGHT TO OSCILLATION HEIGHT, H_{OZ}/H OF THE TEST OBJECT 2 SPRING 1 $IS = 0.30\text{ m}$.

H [mm] \ T [s]	0.70	1.00	1.25	1.50	1.75
60	.016	.057	.059	.055	.041

TABLE XIV.
RATIO OF WAVE HEIGHT TO OSCILLATION HEIGHT, H_{OZ}/H OF THE TEST OBJECT 2 SPRING 2 $IS = 0.27\text{ m}$.

H [mm] \ T [s]	0.70	1.00	1.25	1.50	1.75
60	.030	.067	.067	.018	.006

primary observations of the behaviour of the test object, increasing oscillation heights are also expected for rising wave heights.

- Spring two:

- s_0 : $H_{OZ}/h = 0.016 - 0.059$
- s_1 : $H_{OZ}/h = 0.006 - 0.067$

Overall, both test objects show the same behaviours for the same parameters. The oscillation of the cone is significantly smaller than the circular plate. But, the surface of the two objects must be taken into account. The 30 cm diameter of the plate is more than twice as large as the 14 cm diameter of the cone. Also, it appears that the oscillation of the cone decreases more with increasing submergence depth.

Error associated to the tests on the object two (the cone) appears to be larger, primarily due to the setup of the cone and uncertainty in its movement on the shaft and possibly the slight change in mass of 3.5%.

Further results of these experiments and discussion can be found in [19]. Discussion on wave diffraction by a submerged disc can be found in, for example, [25] and [26].

V. CONCLUDING REMARKS

Laboratory experiments are conducted to study motion of submerged objects under the action of surface waves in shallow and intermediate waves. Although oscillation of the submerged object has a prime application in the above wave energy device, heaving disc are also used for other type of wave energy devices, wave breaker, and the offshore industry. These preliminary experimental results provide an insight into wave-induced oscillations of submerged objects.

The aim of this study is to determine the oscillation behaviour of various forms of submerged primer movers. This is accomplished experimentally in a wave flume and under the influence of water waves and various submergence depth, wave period, wave height and spring stiffness. A systematic approach is used to detect the motion of the object and report the oscillation heights.

For the circular plate and for the cone, the object oscillation increases with increasing wave height and, for the most parts, with increasing wave period. Whereas with increasing submergence depth the object oscillation decreases. Increasing the spring stiffness reduces the oscillation height, as expected. Generally, smoother oscillations are observed with stiffer spring. While wave height seem to have a linear impact on the oscillations,

both wave period and spring stiffness must be considered to determine the oscillations and these appear to be dependent. In addition, it can be observed that the oscillation of the circular plate is greater for the same test parameters than the oscillation of the cone.

The error range associated to the measurement of the oscillation heights was calculated during the analysis of the experiments. About 90% of the test values show an error of 4 – 20%. The deviations increase with increasing wave height. It is recommended to carry out further tests with the test object cone in order to have more comparable data with the plate. In relation to the cone, the basic behaviour should also be observed with a larger dimensioning and a larger difference between the upper and the bottom diameter.

ACKNOWLEDGEMENTS

Authors are grateful to Mr. John Anderson and Mr. Cameron Anderson, technicians of the School of Science and Engineers of the University of Dundee, for the assistance received during the course of the experiments.

REFERENCES

- [1] W. E. Council, *World Energy Resources 2013 Survey*. World Energy Council, 2013.
- [2] R. Pelc and R. M. Fujita, "Renewable energy from the ocean," *Marine Policy*, vol. 26, no. 6, pp. 471–479, Nov. 2002.
- [3] A. Clement and P. McCullen, "Wave energy in europe: Current status and perspectives," vol. 6, pp. 405–431, Oct. 2002.
- [4] H. Erik Friis-Madsen and S. Parmegiani, "Wave dragon," Online, Accessed on: February, 02, 2019. Available: <http://stateofgreen.com/files/download/612>, 2012.
- [5] M. Hayatdavoodi, R. C. Ertekin, and J. T. Thies, "Conceptual design and analysis of a submerged wave energy device in shallow water," in *ASME 36th International Conference on Ocean, Offshore and Arctic Engineering*. American Society of Mechanical Engineers, OMAE, Trondheim, Norway, 2017, p. V010T09A033.
- [6] M. Hayatdavoodi and R. C. Ertekin, "Wave forces on a submerged horizontal plate. Part I: Theory and modelling," *Journal of Fluids and Structures*, vol. 54, no. April, pp. 566–579, DOI: 10.1016/j.jfluidstructs.2014.12.010, 2015.
- [7] —, "Wave forces on a submerged horizontal plate. Part II: Solitary and cnoidal waves," *Journal of Fluids and Structures*, vol. 54, no. April, pp. 580–596, DOI: 10.1016/j.jfluidstructs.2014.12.009, 2015.
- [8] M. Hayatdavoodi, J. Wagner, J. Wagner, and R. Ertekin, "Vertical oscillation of a horizontal submerged plate," in *31st International Workshop on Water Waves and Floating Bodies (IWWFB31)*, Plymouth, MI, USA, 2016, pp. 53–56.
- [9] J. J. Wagner, J. R. Wagner, and M. Hayatdavoodi, "Hydrodynamic analysis of a submerged wave energy converter," in *Proc. 4th Marine Energy Technology Symposium, METS2016, Washington, D.C., USA, April 25-27, 5 p.*, 2016.
- [10] S. Li, "Structual analysis of a wave energy device," Master's thesis, University of Dundee, School of Science and Engineering, mar 2017.
- [11] S. Li, M. Hayatdavoodi, and R. C. Ertekin, "Decoupled hydroelastic analysis of a submerged wave energy device," *Journal of Marine Science and Application*, vol. paper submitted, 2019.
- [12] P. A. Martin and L. Farina, "Radiation of water waves by a heaving submerged horizontal disc," *Journal of Fluid Mechanics*, vol. 337, pp. 365–379, 1997.
- [13] R. W. Carter and R. C. Ertekin, "Focusing of wave-induced flow through a submerged disk with a tubular opening," *Applied Ocean Research*, vol. 47, pp. 110–124, 2014.
- [14] J. N. Newman, "Amplification of waves by submerged plates," *30th International Workshop on Water Waves and Floating Bodies (IWWFB)*, Bristol, UK, pp. 153–156, 2015.
- [15] J. Duffett, R. F. Beck, X. Zhang, K. J. Maki, and J. N. Newman, "Experimental and numerical study of waves amplified by a submerged plate," in *Proceedings of the 31st Int. Workshop on Water Waves and Floating Bodies (IWWFB), 3-6 April, Plymouth, MI, USA*, 2016, pp. 37–40.
- [16] C. Liu, Z. Huang, and W. Chen, "A numerical study of a submerged horizontal heaving plate as a breakwater," *Journal of Coastal Research*, vol. 33, no. 4, pp. 917–930, 2017.
- [17] Y. S. Yu and F. Ursell, "Surface waves generated by an oscillating circular cylinder on water of finite depth: theory and experiment," *Journal of Fluid Mechanics*, vol. 11, no. 4, p. 529551, 1961.
- [18] M. G. Liguo Wang, Jens Engstrom and J. Isberg, "Constrained optimal control of a point absorber wave energy converter with linear generator," *Journal of renewable and sustainable energy*, vol. 7, p. 4, Mar. 2015.
- [19] L. Eckel, "Laboratory experiments of wave interactions on submerged oscillating bodies," Bachelor's Thesis, May 2018.
- [20] P. Schmitt and B. Elsaesser, "A review of wave makers for 3d numerical simulations," in *Marine 2015 6th International Conference on Computational Methods in Marine Engineering*, 2015.
- [21] MathWorks, "Convert rgb colors to hsv - matlab rgb2hsv - mathworks deutschland," Nov. 2018. [Online]. Available: <https://de.mathworks.com/help/matlab/ref/rgb2hsv.html>
- [22] F. Madhi, M. Sinclair, and R. Yeung, "The berkeley wedge: an asymmetrical energy-capturing floating breakwater of high performance," vol. 9, pp. 5–16, 01 2014.
- [23] M. Hayatdavoodi, K. Treichel, and R. C. Ertekin, "Parametric study of nonlinear wave loads on submerged decks in shallow water," *Journal of Fluids and Structures*, vol. 86, pp. 266 – 289, DOI: 10.1016/j.jfluidstructs.2019.02.016, 2019.
- [24] B. Le Méhauté, *An introduction to hydrodynamics and water waves*. Springer Science & Business Media, 2013.
- [25] M. Hayatdavoodi, B. Seiffert, and R. C. Ertekin, "Experiments and calculations of cnoidal wave loads on a flat plate in shallow-water," *Journal of Ocean Engineering and Marine Energy*, vol. 1, no. 1, pp. 77–99, DOI: 10.1007/s40722-014-0007-x, 2015.
- [26] M. Hayatdavoodi, R. C. Ertekin, and B. D. Valentine, "Solitary and cnoidal wave scattering by a submerged horizontal plate in shallow water," *AIP Advances*, vol. 7, no. 6, p. 065212, 2017.